Computers & Geosciences 105 (2017) 10–20

Contents lists available at ScienceDirect

Computers & Geosciences

journal homepage: www.elsevier.com/locate/cageo

Reconstructing daily clear-sky land surface temperature for cloudy regions from MODIS data

Liang Sun[a,b,*], Zhongxin Chen[a], Feng Gao[b], Martha Anderson[b], Lisheng Song[c], Limin Wang[a], Bo Hu[d], Yun Yang[b]

[a] Key Laboratory of Agri-Informatics, Ministry of Agriculture, Institute of Agricultural Resources and Regional Planning, Chinese Academy of Agricultural Sciences, Beijing 100081, China
[b] U. S. Department of Agriculture, Agricultural Research Service, Hydrology and Remote Sensing Laboratory, Beltsville, MD 20705, USA
[c] School of Geographical Sciences, Southwest University, Chongqing 400712, China
[d] Ningbo Meteorological Bureau, Ningbo 315012, China

ARTICLE INFO

Keywords:
MODIS
Land surface temperature
Reconstruction
Remotely Sensed DAily land Surface Temperature reconstruction (RSDAST) model
TVDI

ABSTRACT

Land surface temperature (LST) is a critical parameter in environmental studies and resource management. The MODIS LST data product has been widely used in various studies, such as drought monitoring, evapotranspiration mapping, soil moisture estimation and forest fire detection. However, cloud contamination affects thermal band observations and will lead to inconsistent LST results. In this study, we present a new Remotely Sensed DAily land Surface Temperature reconstruction (RSDAST) model that recovers clear sky LST for pixels covered by cloud using only clear-sky neighboring pixels from nearby dates. The reconstructed LST was validated using the original LST pixels. Model shows high accuracy for reconstructing one masked pixel with R^2 of 0.995, bias of −0.02 K and RMSE of 0.51 K. Extended spatial reconstruction results show a better accuracy for flat areas with R^2 of 0.72–0.89, bias of −0.02–0.21 K, and RMSE of 0.92–1.16 K, and for mountain areas with R^2 of 0.81–0.89, bias of −0.35−−1.52 K, and RMSE of 1.42–2.24 K. The reconstructed areas show spatial and temporal patterns that are consistent with the clear neighbor areas. In the reconstructed LST and NDVI triangle feature space which is controlled by soil moisture, LST values distributed reasonably and correspond well to the real soil moisture conditions. Our approach shows great potential for reconstructing clear sky LST under cloudy conditions and provides consistent daily LST which are critical for daily drought monitoring.

1. Introduction

Land surface temperature (LST), generally defined as the skin temperature of the Earth's surface, is an important factor in the study of environment, agriculture, hydrology and meteorology. LST reflects the processes of evapotranspiration (ET) (Anderson et al., 2012; Sun et al., 2013), surface energy balance (Bastiaanssen et al., 1998; Su, 2002), soil moisture change (Carlson et al., 1995) and climate change (Jin et al., 2005; Maimaitiyiming et al., 2014).

Land surface temperature can be retrieved using remotely sensed thermal infrared (TIR) data. Two widely used TIR instruments include the Advanced Very High Resolution Radiometer (AVHRR) and Moderate Resolution Imaging Spectrometer (MODIS). Both are capable of observing the earth surface at least once per day at 1 km spatial resolution.

The MODIS instrument is a highly sensitive radiometer operating in 36 spectral bands ranging from 0.4 μm to 14.4 μm. MODIS is operating onboard Terra and Aqua. Terra was launched in December 1999 and Aqua in May 2002. A ± 55° scanning pattern at 705 km altitude achieves a 2330 km swath that provides global coverage every one to two days. Aqua has a 1:30 am/pm equator crossing time while Terra has a 10:30 am/pm equator crossing time. Thus, daytime MODIS thermal band imagery are available locally once in the morning from TERRA and once in the afternoon from AQUA. The MODIS team has developed and published more than 20 atmospheric, oceanic and land surface data products. The MODIS LST product is retrieved using the generalized split-window algorithm (Wan and Dozier, 1996) and the day/night algorithm (Wan, 1997). The reported error in LST is less than 1k, as validated over homogenous land surface patches (Wan et al., 2002). As a high quality data product, MODIS LST has been widely applied in many fields, especially drought monitoring. Many remote sensing drought monitoring indices are developed based on

* Corresponding author at: U. S. Department of Agriculture, Agricultural Research Service, Hydrology and Remote Sensing Laboratory, 10300 Baltimore Avenue, Beltsville, MD 20705, USA.
E-mail addresses: sunliang001@gmail.com, liang.sun@ars.usda.gov (L. Sun).

http://dx.doi.org/10.1016/j.cageo.2017.04.007
Received 12 December 2016; Accepted 24 April 2017
Available online 29 April 2017
0098-3004/

LST, such as Temperature Condition Index (TCI) (Kogan, 1995), Vegetation Health Index (VHI) (Kogan, 1997), Temperature Vegetation Dryness Index (TVDI) (Sandholt et al., 2002; Sun et al., 2012), and the Evaporative Stress Index (ESI) (Anderson et al., 2011, 2013, 2016).

Time-series of land surface parameters are required for continuous modeling and monitoring of environmental phenomena. However, the optical band signal from the land surface cannot penetrate clouds. When a pixel is contaminated by cloud, land surface information may be mixed with or totally blocked by the cloud. In reality, cloudy-sky conditions represent more than half of the actual day-to-day weather around the globe (Jin, 2000), which means we would lose half the information regarding land surface conditions if cloudy areas are excluded during analysis.

For the purpose of time-series LST monitoring, a robust daily LST gap filling algorithm is required for prolonged periods with overcast skies, when satellite-derived LST measurements are not available (Westermann et al., 2011). However gap-filling for LST is more difficult than for reflectance because LST is affected by various environment factors such as solar radiation, air temperature, land cover, soil moisture. Few research studies have focused on reconstructing LST under cloud cover conditions. Those that have been conducted can be divided into two groups. The primary intentions of the first group are to reconstruct LST under cloud cover, which means the cloud conditions should be considered in the model (Jin, 2000). developed a 'neighboring-pixel approach' on the basis of surface energy balance principle, assuming the temperature difference between a cloudy pixel and its neighboring clear pixel is due to the differences in energy fluxes, i.e., net solar radiation, net longwave radiation, and sensible and latent heat flux between the cloudy and its neighboring pixels (Lu et al., 2011). revised the 'neighboring-pixel approach' by exploiting the temporal domain offered by geo-stationary satellite observations to acquire adequate samplings to capture the diurnal cycle of LST (Zhang et al., 2015). proposed a method for estimating cloudy LST based on a one-dimensional heat transfer equation and the evolution of daily surface temperatures and net shortwave solar radiation (Kou et al., 2016). combined MODIS and AMSR-E data with Bayesian Maximum Entropy method to reconstruct high-quality LST. Recovering real LST under cloud needs additional information under cloud, such as solar radiation or cloudy LST. A complicated physical relationship between clear and cloudy LST is required. The primary intentions of the second group are to reconstruct the clear sky LST, which is not the real LST under cloudy conditions (Neteler, 2010; Metz et al., 2014) used elevation, solar angle, precipitation and temperature as additional variables in the spline interpolation method to reconstruct LST values. These methods rely on climate factors that are difficult to obtain precisely as a spatially distributed map. Errors in the climate variable specifications can lead to large errors in the reconstructed LST, particularly for large area applications (Xu and Shen, 2013). used the Harmonic ANalysis of Time Series (HANTS) algorithm to remove cloud-affected observations and reconstruct the MODIS LST data. However extreme events may not be well characterized.

The reconstructed clear sky LST would be very useful for evaluating drought monitoring indices such as TVDI which is estimated based on the triangle feature space formed by the scatter plots between NDVI and LST images. The triangle space method assumes that a full range of fractional vegetation cover and soil moisture contents is represented in the data and that climate forcings are spatially uniform (Sun et al., 2012). Therefore if there are few valid pixels available in the study area, it is difficult to form a triangle space. In addition, in the triangle space, soil moisture is assumed to be only affected by the LST and NDVI, which means cloud, an extra factor affecting LST, should not be considered in the drought monitoring.

In this study, we developed a new Remotely Sensed DAily land Surface Temperature reconstruction (RSDAST) model to reconstruct gap pixels in the MODIS daily LST product, based on an assumption that the LST difference between nearby pixels is small during a short time period. The RSDAST model is used to recover LST for clear sky condition. The objective of this study is to develop, test and validate the RSDAST model in Northwestern China. The results were evaluated using: (1) masked pixels every 10 days from one year; (2) original clear-sky high quality MODIS LST; and (3) triangle feature space formed by scatterplots between LST and NDVI used for drought index TVDI.

2. Methodology

2.1. Theoretical basis of LST reconstruction model

For two clear-sky neighboring pixels, the LST recorded at the satellite overpass time on day t_0 can be expressed as,

$$LST(x_0, y_0, t_0) = LST(x_1, y_1, t_0) + \varepsilon_0 \quad (1)$$

where (x_0, y_0),(x_1, y_1) are the locations of two nearby pixels, t_0 is observation date, ε_0 is the LST difference between two pixels on day t_0. Because the locations of two pixels (x_0, y_0), (x_1, y_1) are very close, they are most likely under the same weather conditions (such as solar radiation, air temperature and rainfall). For example, if air temperature decreases resulting from rainfall, then the $LST(x_0,y_0,t_0)$ and $LST(x_1,y_1,t_0)$ should decrease synchronously within the area. On the next day, t_1, we can write a similar equation:

$$LST(x_0, y_0, t_1) = LST(x_1, y_1, t_1) + \varepsilon_1 \quad (2)$$

where ε_1 is the LST difference on day t_1. If the land surface is homogenous, both ε_0 and ε_1 should be close to zero. Although, truly homogenous surfaces are rare, which means ε_0 (ε_1) would typically be non-zero, generally $LST(x_0,y_0)$ and $LST(x_1,y_1)$ increase or decrease synchronously, so we can assume that ε_0 is usually close to ε_1 if t_0 and t_1 are close in time.

With this assumption, Eqs. (1) and (2) can be used to derive the following expression:

$$LST(x_0, y_0, t_0) - LST(x_1, y_1, t_0) = LST(x_0, y_0, t_1) - LST(x_1, y_1, t_1) \quad (3)$$

Eq. (3) means the LST difference between two nearby pixels is the same for two closely separated days. It can also be expressed as:

$$LST(x_0, y_0, t_0) - LST(x_0, y_0, t_1) = LST(x_1, y_1, t_0) - LST(x_1, y_1, t_1) \quad (4)$$

Eq. (4) means the LST difference between two days at one location is the same as that at a nearby location.

Then if LST at location (x_0,y_0) is absent at day t_0, it can be calculated as

$$LST(x_0, y_0, t_0) = LST(x_0, y_0, t_1) - LST(x_1, y_1, t_1) + LST(x_1, y_1, t_0) \quad (5)$$

2.2. Reconstruction of missing LST

By introducing additional information from neighboring valid pixels, we compute the LST for a missing central pixel (x_0,y_0) on day t_0 with a weighting function

$$LST(x_0, y_0, t_0) = \sum_{p=t_0-4}^{t_0+4} \sum_{i=1}^{N} W_i \bullet [LST(x_0, y_0, t_p) - LST(x_i, y_i, t_p) + LST(x_i, y_i, t_0)] \quad (6)$$

$$W_i = \frac{1/(D_i \bullet S_i)}{\sum_{i=1}^{N} [1/(D_i \bullet S_i)]}$$

where W_i is a weighting function computed from a distance factor (D_i) and a similarity factor (S_i), p is the day of the comparison image, i is the position of a valid neighboring pixel, and N represents the total number of valid pixels selected from 9×9 pixels window for each date p. We not only use valid pixels from the nearest day, but also from the 8 days surrounding the target reconstruction date to increase sample size. In

Eq. (6), LST(x_0,y_0,t_p) is a valid central pixel on day p and LST(x_i,y_i,t_p) is a valid surrounding pixel on day p. Then [LST(x_0,y_0,t_p) - LST(x_i,y_i,t_p)] is defined as the LST Difference of Pixel Pair (LDPP). Each LDPP in 9×9 pixels window from the nearest 8 days is assigned a weight used in estimating the gap LST.

2.2.1. Distance factor

According to the first law of geography, everything is related to everything else, but near things are more related than distant things (Tobler, 1970). In another words, the closer two pixels' are, the more similar their LST values should be. So the closer pixel gets to the central position, with spatial distance D_i calculated as:

$$Di = \sqrt{(x_i - x_0)^2 + (y_i - y_0)^2} \quad (7)$$

the larger the weight assigned to that pixel pair.

2.2.2. Similarity factor

Similarity factor is proposed to identify the neighboring pixel with the most similar surface conditions to the central pixel which needs to be gap-filled. The difference of LST is considered to describe the surface conditions similarity. The smallest LST difference represents the most similar conditions. Since the central pixel on date t_0 [LST(x_0,y_0,t_0)] is invalid/gap, based on Eq. (3) that LST difference between two nearby pixels is the same for two closely separated days, the LDPP on date t_p is used to identify the pixel with the most similar conditions. Thus the smallest LDPP reflects the closest conditions of two nearby pixels, which is assigned as the largest weight. The similarity factor S_i is calculated as

$$S_i = |LST(x_0, y_0, t_p) - LST(x_i, y_i, t_p)| + 1 \quad (8)$$

In the reversed weighting function Eq. (6), a smaller S_i means similar land surface conditions, and thus a higher weight will be assigned in the LST prediction model. S_i value starts from "1" to avoid "0" similarity factor when two temperature values are identical.

2.3. LST reconstruction steps

The main processing steps of the LST reconstruction algorithm are illustrated in Fig. 1. When the program finds a missing LST pixel on day t_0, it extracts all the valid LST(x_0,y_0,t_p) within a 9×9 pixel window from the nearest 8 days, and then calculates the total weight W_i for each pixel pair. The missing LST value is computed using Eq. (6), which is then restored to the grid as a valid value for the processing of the next pixel.

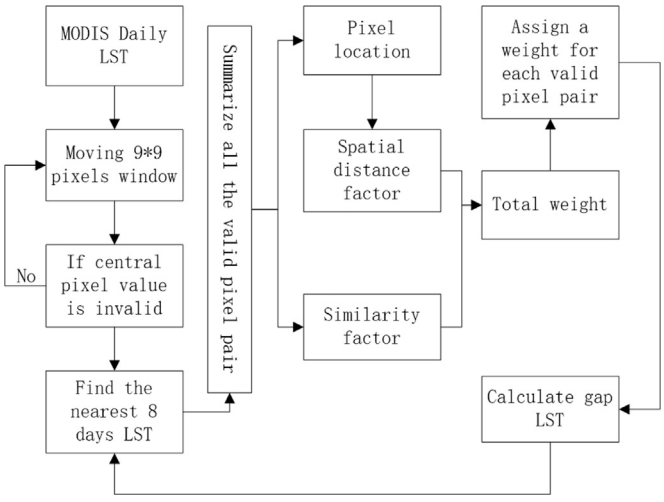

Fig. 1. Flowchart describing the LST reconstruction model.

2.4. Validation strategies

Since the intent of this paper is to reconstruct the clear-sky LST in cloudy regions (rather than the actual cloud effected LST), it is not appropriate to compare the reconstructed LST with that from ground-based measurements which are cloud effected. Accordingly, two validation strategies are proposed as follows: (1) In order to test the model reconstruction performance on one fixed pixel, two pixels are masked every 10 days in 2002. One is covered by crop and another is covered by forest (location shown in Fig. 2). The reconstructed LST value is then compared with the original MODIS LST. In total, there are seven days of valid crop pixels and 13 days of valid forest pixels; (2) In order to test the model performance in terms of spatial reconstruction capabilities, two large regions were artificially masked in the original MODIS images, as shown in Fig. 2. One area is located in the plain with little heterogeneity including 18913 km^2, and the other is located in a mountainous region with complex terrain and strong heterogeneity in LST, including 13009 km^2. Three dates in different season from 2000 to 2002 were selected for each target area to capture locally clear-sky conditions.

3. Study area and data

3.1. Study area

The study area is located in Northwest China as shown in Fig. 2, covering the coordinate range between 91.7°E –112.2°E, 30.7°N –43.1°N, including Gansu, Ningxia, Shaanxi provinces and part of Inner Mongolia, Qinghai and Sichuan provinces. Precipitation and temperature are strongly variable over this area, resulting in a range in climate types, from arid and semiarid to humid subtropical. The terrain of this area is complicated, and includes plain, desert, highland and mountain regions, with an elevation range from 50 to 5000 m. The western part of the study area is part of the Tibetan Plateau, which is considered as the third pole of the earth, with elevations from 3000 to 5000 m. The elevation of the east area is relatively low, and the lowest area is located in the middle eastern part of the study area called the 'Guanzhong Plain'. The terrain is relatively flat in this plain and includes cultivated crops.

3.2. MODIS data

In this study, we downloaded Collection 5 MODIS TERRA LST products (MOD11A1) at 1 km resolution for the years 2000–2002 and 2014. The MODIS LST from 2000 to 2002 were used to develop method and validate results. The 2014 MODIS LST data were used to investigate the impacts of precipitation and irrigation (precipitation and irrigation records at the forest and crop site were only available for 2014). Only daytime LST (about 10:30 am) was chosen as the testing target in this study. Four MODIS tiles (h25v04, h25v05, h26v05 and h27v05) were selected to cover all the study area. We used the MRT (MODIS Reprojection Tool) to mosaic and resample all the MODIS product data to 1 km grid. A sub-image of 1678×1345 pixels was then extracted from all data products.

Cloud contaminated pixels have been excluded from the MODIS LST product (Ackerman et al., 1998). However, effects of cloud edges on LST may remain in the product. The LST quality around the cloud edges is relatively lower as indicated by the MODIS LST Quality Control (QC) flags. Therefore, in this paper, we only use good quality LST pixels recognized by QC flags to reconstruct because low quality pixels would introduce extra errors in the model.

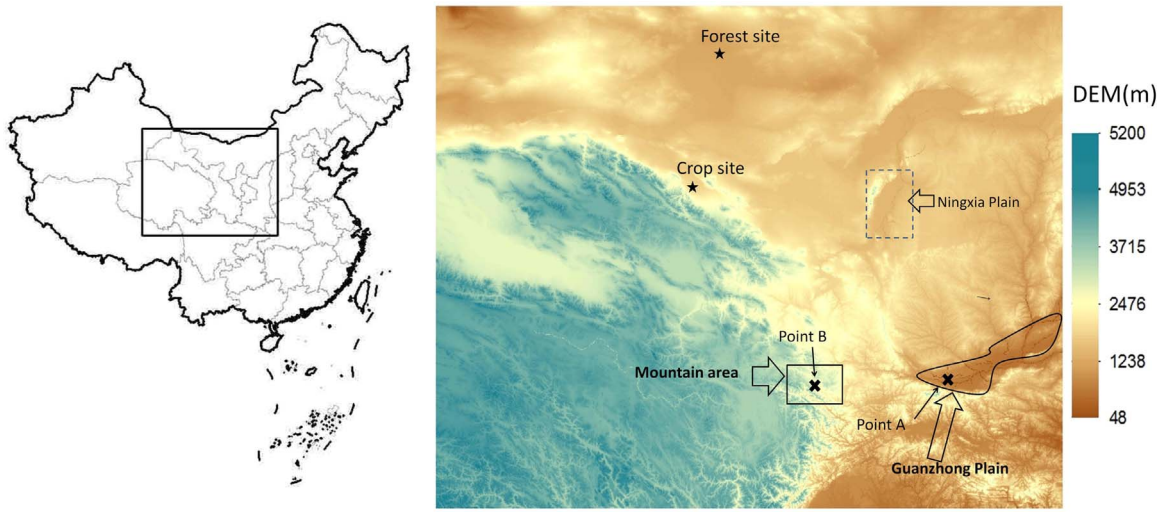

Fig. 2. Map of the study area. Right panel shows a digital elevation model (DEM, m). The two stars indicate crop and forest sites used for validation. The two X's (A and B) are used for LST time series extraction. Point A is located in the plain and point B is on a mountain slope. Two areas (mountain area and Guanzhong Plain) enclosed by lines are also used for model validation.

4. Results

4.1. Model assumption verification

The model assumes that the LST difference between nearby pixels is similar over short time periods. To verify this assumption, we used the MODIS daily LST product collected over the study area for 2001 to calculate the temperature difference (TD) between the center pixel and the averaged value from 8 surrounding pixels. The TD image was generated for each day. Then the standard deviation and the mean absolute value of the TD annual time series for each pixel were computed, as shown in Fig. 3a and c. The results show that the standard deviation and the mean absolute value of TD have a strong correlation with the distribution of the slope of terrain. The north and east area is relatively flat, therefore the TD standard deviation of these areas is below 1 K, and the mean absolute value is below 0.5 K, indicating that there is little seasonal TD variation for these areas. Even though the west is mountainous, with varying topography, the standard deviation of the 2001 TD time series for most of this area is still under 2 K and the mean absolute value is under 1.5 K. Large standard deviations up to 4 K and large mean absolute value up to 2.5 K are observed only in a small area located in the southwest with extremely variable topography. This confirms our assumption that the difference of LST between a pixel and the surrounding pixels are similar during the time series even for the entire year. In comparison, the LST timeseries show strong variability over the same time period (Fig. 3b), due to seasonal variations in solar radiation and climate. Most pixels vary from 5 to 21 K much greater than that of TD. The standard deviation in LST is more correlated with latitude than with topography, with the northern area showing larger LST seasonal variation. The TD and LST behavior of point A and B (the location is shown in Fig. 2) is exemplified in the timeseries in Fig. 4. There is little

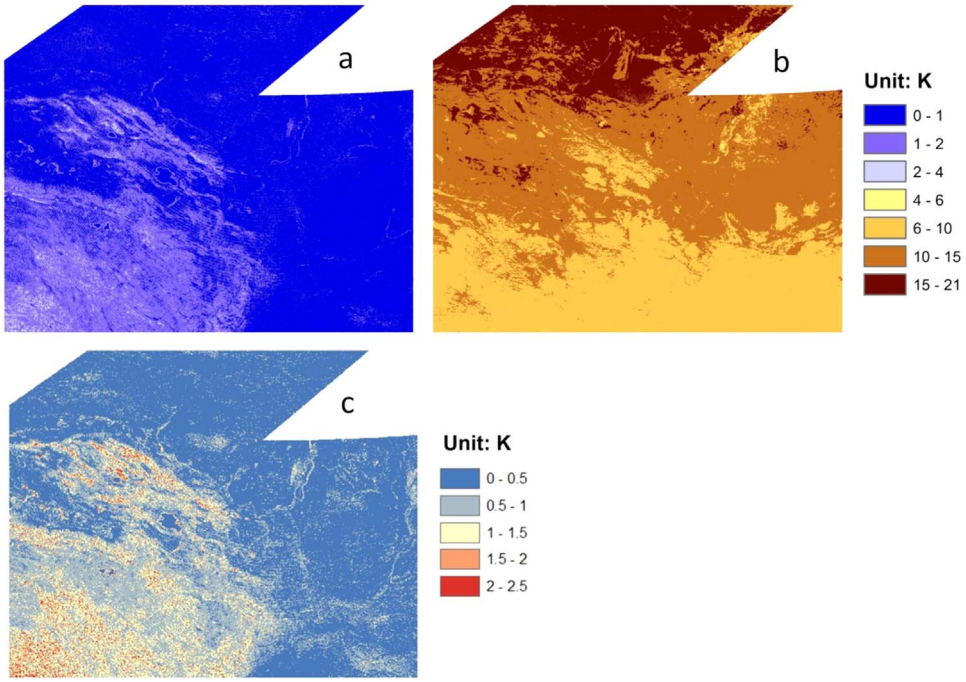

Fig. 3. Spatial distribution of standard deviation of the TD time series (a) and the LST time series (b), and the mean absolute value of TD for each pixel (c) of 2001 over the study area.

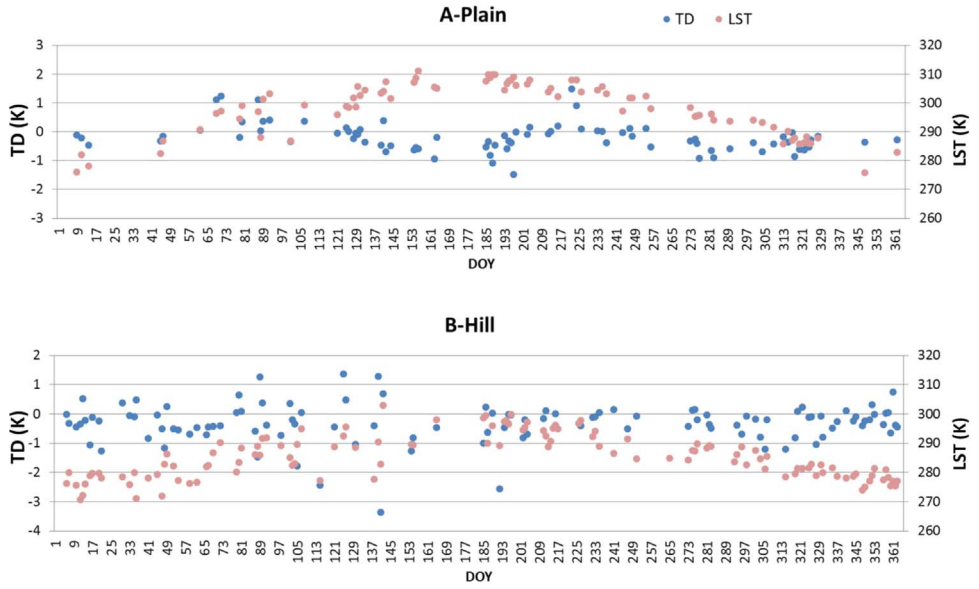

Fig. 4. LST (right axis) and TD (left axis) from 2001 time series at point A and B (shown in Fig. 2). Point A is located in plain area and point B is located in mountain area.

seasonal variation for the TD time series which is relatively stable and close to zero for the whole year, but there is strong variation for LST.

4.2. Validation using MODIS original LST

First, the reconstructed LST was validated using the first strategy described in Section 2.4. Fig. 5a shows the scatter plots between reconstructed and original MODIS LST. The reconstructed LST shows very high accuracy with R^2 of 0.995, bias of −0.02 K and RMSE of 0.51 K. The forest site is located in an extremely arid region, with precipitation of less than 50 mm per year and potential evaporation of approximately 3755 mm per year (Li et al., 2013), resulting in higher LST compared with the crop. Fig. 5b and c show the difference between the reconstructed and original LST on each valid date over two sites. The difference on most days is between −0.5 and 0.5 K. Even though the largest error is around ±1 K, it is still a reasonable error. We checked the images with relatively large errors such as DOY 230 for the forest site and DOY 240 for the crop site, and found that there is cloud

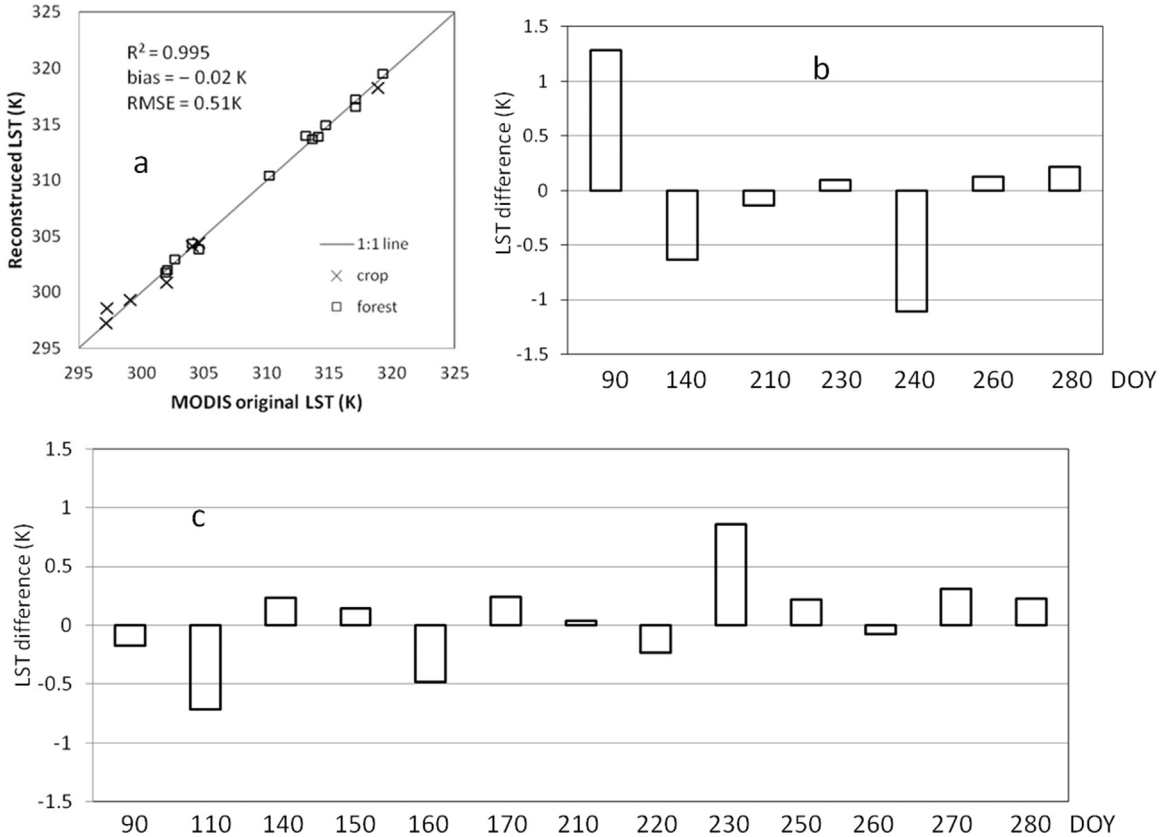

Fig. 5. Scatter plots between original MODIS LST and reconstructed LST over two sites (a); LST difference between reconstructed and original LST (reconstructed LST- original LST) at the crop site (b); and the forest site (c).

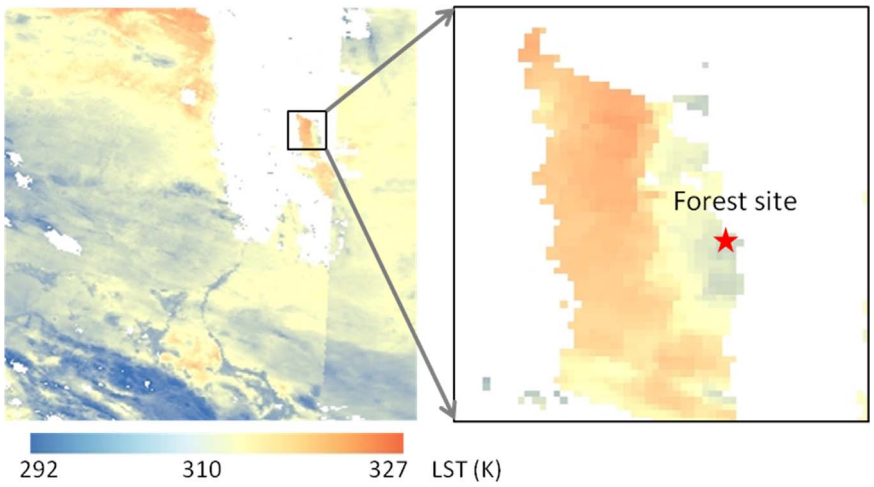

Fig. 6. LST image filtered by good quality flag on DOY 230 of 2014. Red star shows the location of the forest site. White area represents the cloud mask.

Table 1
Error statistics between original and reconstructed LST for plain and mountain areaS.

region	Year	DOY	Correlation coefficient (R)	Bias (K)	RMSE (K)
plain	2000	086	0.72	0.21	1.00
18913 pixels	2001	196	0.87	0.10	0.92
	2002	151	0.89	−0.02	1.16
mountain	2001	105	0.89	−0.35	1.42
12997 pixels	2001	318	0.83	−0.43	1.61
	2002	274	0.81	−1.52	2.24

effect around the sites on these two days. Although we have excluded the low quality pixels as Section 3.2 described, it is difficult to ensure that all the pixels are 100% clear. Fig. 6 shows the LST pixels extracted only from good quality data on DOY 230. The forest site is located right next to the cloud mask edge, where the temperature is obviously affected by cloud. For the crop site on DOY 90, we found that there was an irrigation event on that day, which may result in heterogeneous land surface conditions responsible for the relatively large LST reconstruction errors.

In order to test the model performance in terms of spatial reconstruction capabilities, two regions were artificially masked in the clear-sky MODIS images, as shown in Fig. 2, so the algorithm in this case uses only data from proximate days to fill in gaps (referred as masked area). The gap-filled results were used to compare with the original LST from the masked area. One area is located in the plain with little heterogeneity, and the other is located in a mountainous region with complex terrain and strong heterogeneity in LST. Three images in different seasons from 2000 to 2002 were selected for each target area to capture the local clear-sky conditions (Table 1). Fig. 7 shows scatter plots comparing original and reconstructed LST for each area and date, demonstrating distributions close to the 1:1 line. The performance over the plain (Fig. 7a-c) is better than over the mountain area (Fig. 7d-f). As shown in Table 1, the bias and RMSE for all three days found for the plain area were small, with bias ranging from −0.02–0.21 K and RMSE from 0.92–1.16 K. R^2 values are lowest for DOY 86 of 2000, due in part to a lower range of variability in LST on

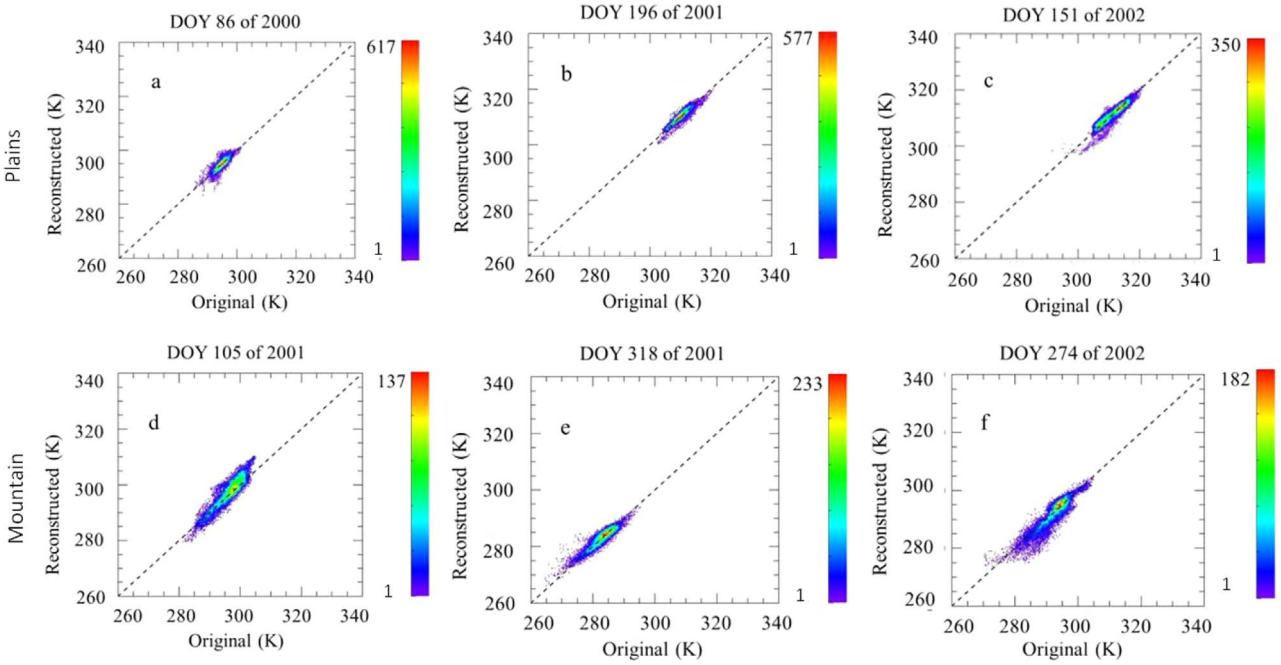

Fig. 7. Scatter plots between original LST and reconstructed LST for different days. The color bar shows the point density. The first row corresponds to plain area, and the second row corresponds to the mountain area.

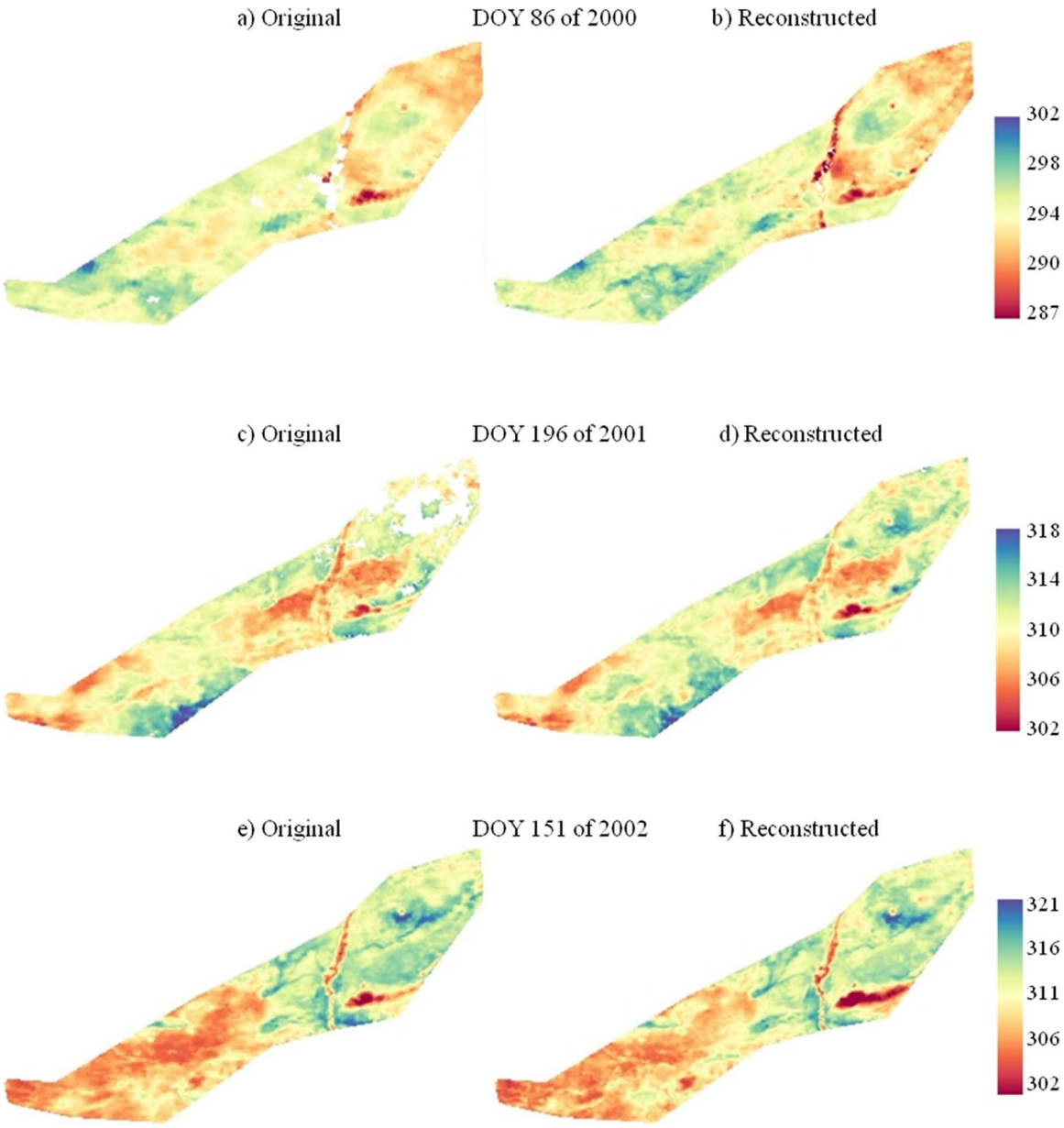

Fig. 8. Original (a, c, e) and reconstructed MODIS LST (b, d, f) for the plain area on DOY 86 of 2000, DOY 196 of 2001 and DOY 151 of 2002.

that day (Fig. 7a). Fig. 8 shows maps of the original and reconstructed LST values, demonstrating capabilities of RSDAST to reconstruct spatial temperature features in the landscape. A river system flowing from west to east is clearly shown on the reconstructed image (Fig. 8b, d, f), with lower LST values (305 K) in comparison with the surrounding area (about 310 K on average).

While the bias and RMSE for the mountain area exceed those for the plain, the correlations are strong (R^2 greater than 0.8 for all the three days) due to the larger range in LST over this more complex landscape. RMSE ranges from 1.42 to 2.24 K. Although the accuracy over the mountain area is not as good as that of the plain area, it is still comparable to other LST reconstruction methods. For example Jin (2000) reported the RMSE of 1.5–3.2 K (Jin, 2000) and Lu et al. (2011) reported about 5 K (Lu et al., 2011). The relatively lower accuracy over this area reflects the fact that the TD variation over a heterogeneous surface is larger than that for a homogenous surface (see Figs. 3 and 4). Fig. 9 shows the original and reconstructed LST distributions over the mountain area for three dates. The reconstruction model not only captures the main LST distribution, but also recovers spatial details, such as the ridge and the valley, which are clearly displayed in the reconstructed image (Fig. 9b, d and f).

4.3. Spatial distribution of reconstructed LST

We reconstructed the MODIS LST based on the good quality, using data from 2014 over the study area. Images from two days were selected to demonstrate the capabilities of RSDAST as it would be applied in practice (Figs. 10 and 11). The reconstructed LST greatly increased the available pixels. Especially for DOY 190, there are too few valid pixels left in the original LST image (Fig. 11a) to be applied in any monitoring applications. The reconstructed LST (Fig. 11b) gap filled most of the area and has a similar spatial pattern with NDVI (Fig. 11c). The mainly terrain features were also correctly reconstructed by the model. The mountain area in the southwest, Guanzhong Plain in the east, and the Qinghai Lake could all be recognized clearly.

It is difficult to validate the reconstructed LST in the gap area, since the reconstructed LST value is not the real LST which can be measured. Given the fact that a triangle feature space would be formed by the

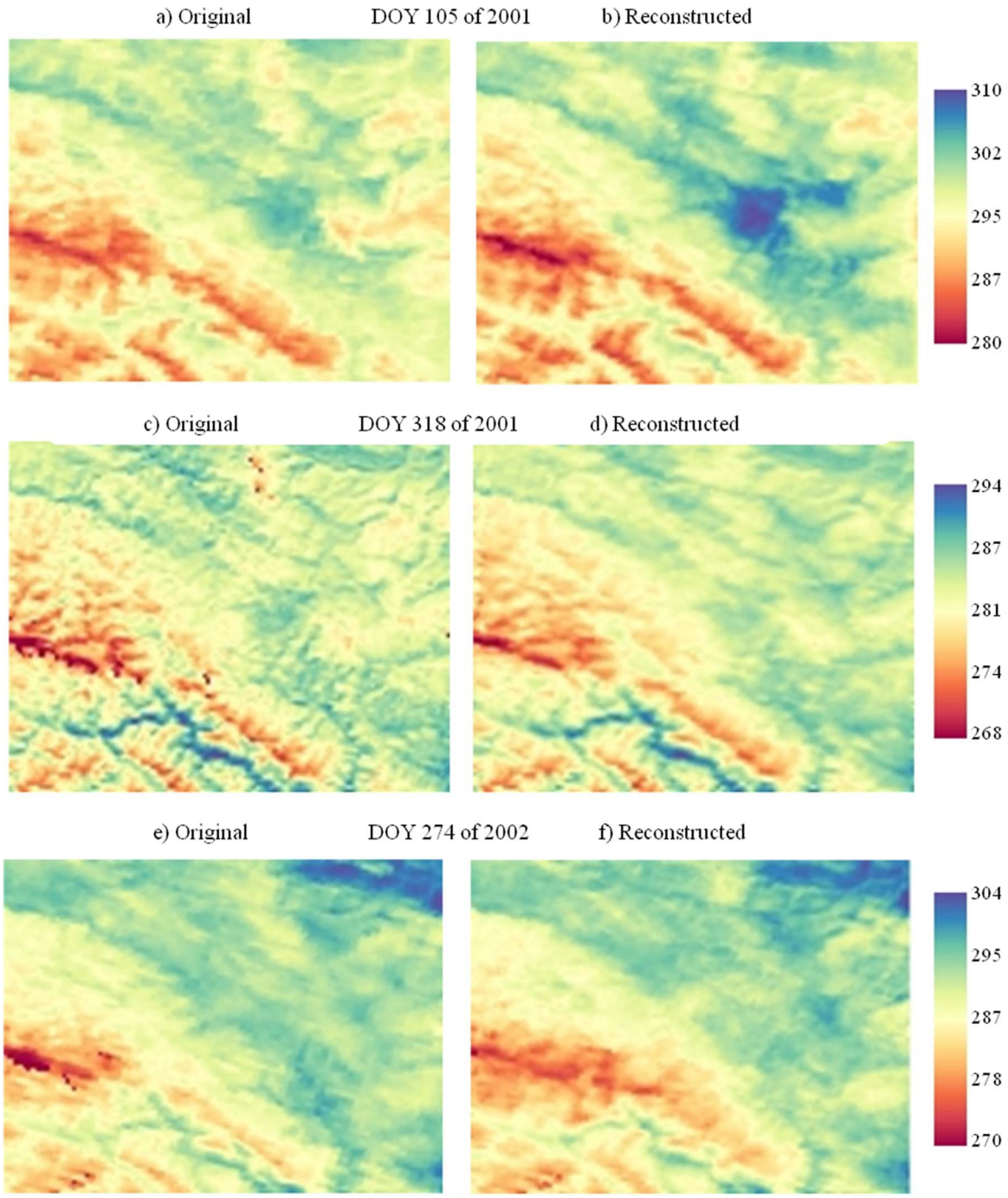

Fig. 9. Original (a, c, e) and reconstructed LST (b, d, f) for mountain area on DOY 105 of 2001, DOY 318 of 2001 and DOY 274 of 2002.

scatter plots between LST and NDVI images over an area under clear sky (Sandholt et al., 2002; Sun et al., 2012), the reasonableness of the reconstructed LST spatial pattern could be checked by the pattern of the triangle feature space. To avoid the effect of terrain on LST, the area confined by the white box in Figs. 10 and 11 was selected to develop scatter plots shown in panels (d) and (e). For DOY 172 as Fig. 10 shown, the scatter plots from the reconstructed LST forms a much better triangle space than the scatter plots from the original LST. Furthermore, in the triangle space, the points from the reconstructed pixels correspond very well with the original points. This indicates that the LST is mainly controlled by soil moisture, and that the reconstructed LST is under the same clear sky conditions as the original LST. For DOY 190 as Fig. 11 shown, there is no pixels in the confined area from original LST, whereas the scatter plots from the reconstructed LST formed a clearly triangle space. The points with low LST and high NDVI on the right side of the triangle space correspond to the Ningxia Plain, which is dominated by irrigated crops in the middlewest of the confined box, indicating a reasonable spatial distribution of reconstructed LST. However, a small fraction of unfilled pixels remain in each of the two reconstructed images (Figs. 10b and 11b) due to a lack of valid central pixels from the nearest 8 days.

5. Discussion

Comparing to other gap-filling methods (Metz et al., 2014; Neteler, 2010; Xu and Shen, 2013), RSDAST is more flexible in using ancillary LST images from nearby days. No other climate variable inputs are required, such as solar radiation and temperature, the spatial distribu-

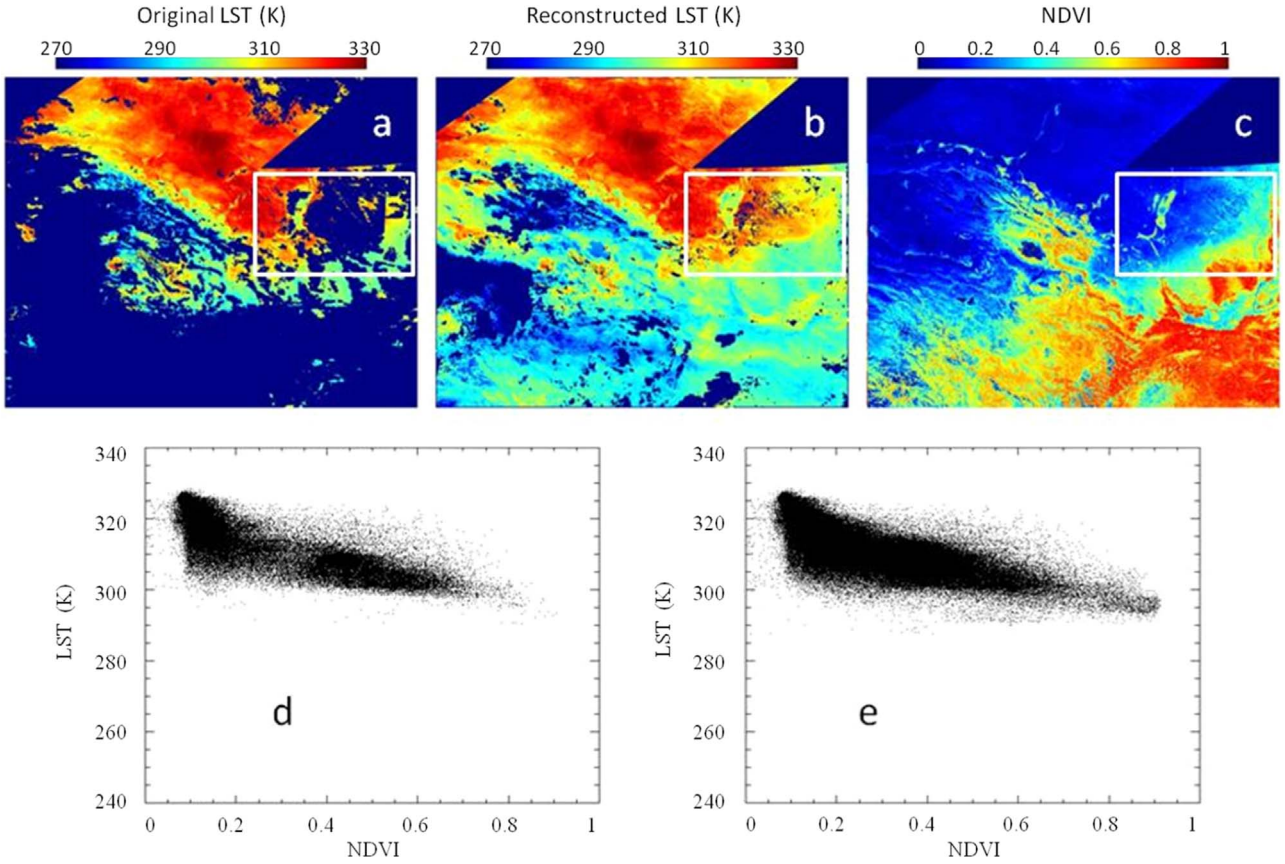

Fig. 10. MODIS original LST (a), reconstructed LST (b), NDVI (c), scatterplots between NDVI and original LST (d), and scatterplots between NDVI and reconstructed LST (e) on DOY 172 of 2014.

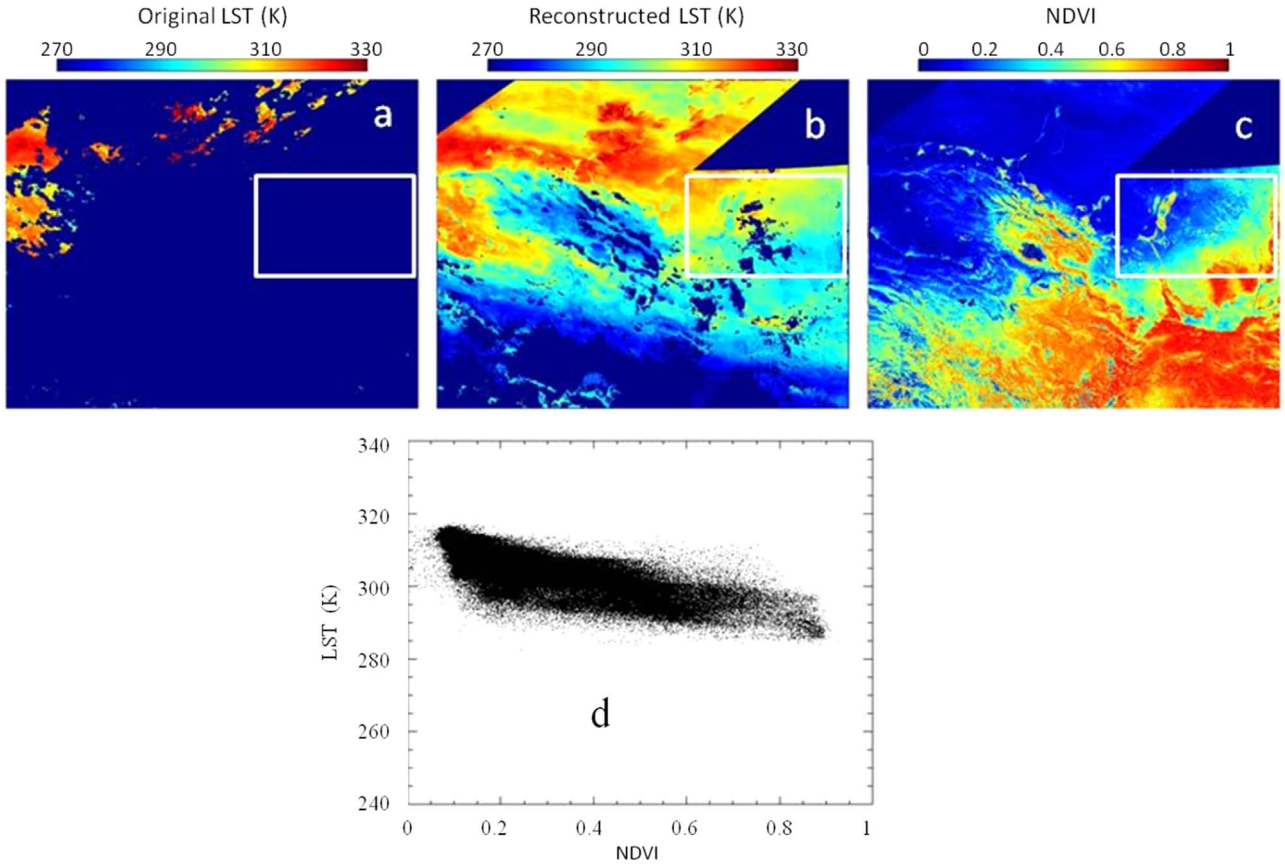

Fig. 11. MODIS original LST (a), reconstructed LST (b), NDVI (c), and scatterplots between NDVI and reconstructed LST (d) on DOY 190 of 2014.

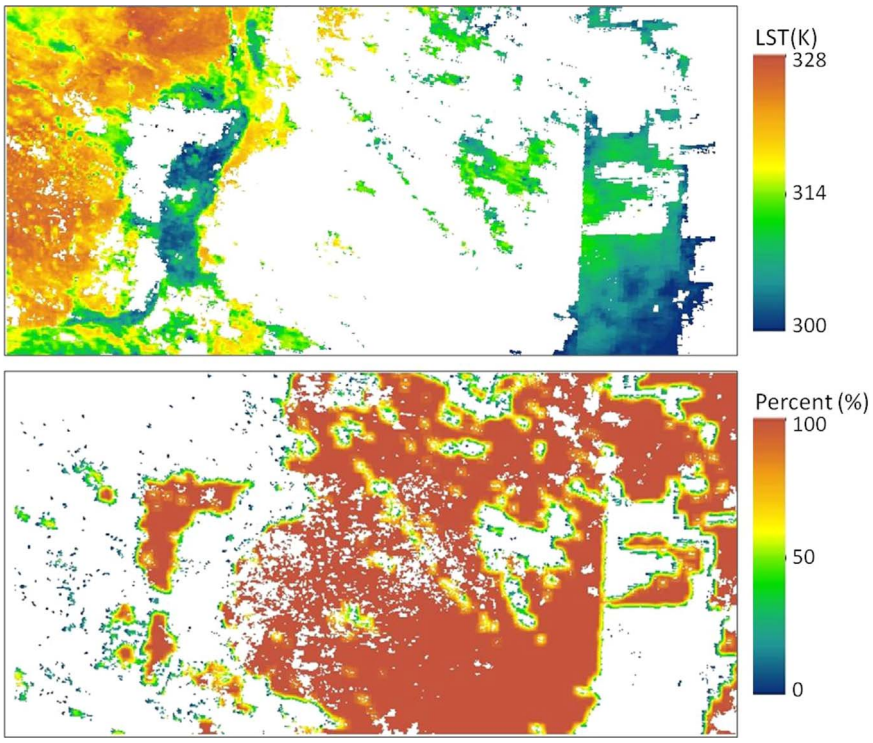

Fig. 12. The original LST (top) and the percentage of the reconstructed pixels used in the gap-filling at each pixel (bottom) on DOY 172 of 2014 (Corresponding to the confined area in Fig. 10). The white in top figure represents missing/gap pixels. The white in bottom figure shows valid pixels that do not need to gap-fill.

tion of which are difficult to ascertain. The principle of RSDAST is conceptually simple and a major strength is the use of both spatial and temporal information from valid clear pixels close to the gaps. Meanwhile, the LST Difference of Pixel Pair is used to find the most appropriate and relevant pixels, which promotes spatial and temporal continuity within the filled results. There is a great potential to use RSDAST to generate spatially and temporally continuous soil moisture conditions and then evapotranspiration mapping (Sun et al., 2012, 2013). In this study, RSDAST showed good performance when applied to MODIS LST products. The approach may be also extended to other sensors, such as NOAA-AVHRR and VIIRS, because the model only requires LST as inputs. However, several factors need to be considered when applying the approach to other areas or sensors.

5.1. Cloud effects

The MODIS cloud mask algorithm uses a series of visible and infrared threshold tests to determine the confidence in which the satellite's view of the Earth's surface is unobstructed by clouds. If clouds are present, then LST data will not be available for the location (http://modis-atmos.gsfc.nasa.gov/). However, effects of cloud edges such as cloud shadows have a very substantial impact on satellite land products. They degrade the quality of clear-sky composite products and may introduce systematic biases in long-term data records (Khlopenkov and Trishchenko, 2007). Although only pixels flagged by good quality were chosen to reconstruct, sometimes it also fails to detect some serious cloud shadows (Luo et al., 2008). In our study, as Fig. 6 shown, cloud effect could also be found on the edge of the cloud mask. Apparently, this effect would bring errors in the model.

5.2. View time and view angle

Terra/MODIS overpass times vary and the exact image acquisition time could be a little different every day. For example, the overpass time of Terra at the crop site in this study varied from 10:00 to 12:00 (different swaths) even during an 8-day period. This may introduce errors when the samples selected from the nearest 8 days are actually observed at different times of day, even over only a hours. Another possible source of error is differences in view angle. View angles in the MODIS LST product over an 8-day period can vary within ± 55°. Wan et al. (2002) has pointed out that 1-km MODIS LST is underestimated by −1.6 to −3.1 K at different viewing angles under different atmospheric conditions. In addition to angular effects, the size of pixel's footprint varies from nadir to off-nadir view. The footprint of 1-km resolution pixel may not same within the reconstruction period, which will introduce some uncertainties in the reconstructed LST.

5.3. Reconstruction distance

If only the original valid pixels are used as samples to reconstruct LST, this can limit the number of pixels that are reconstructed successfully. In order to reconstruct as many LST pixels as possible, the reconstructed pixels are also used as valid samples in the search window for nearby pixels. For an area with large gap, the quality of samples based on the reconstructed pixels may not be as good as the original retrievals, and the reconstructed image quality may reduce as the filled distance from original valid pixels getting further. Fig. 12 shows the percentage map of the reconstructed pixels that were re-used in the gap-filling for DOY 172 of 2014. The area corresponded to the confined area in Fig. 10. The percentage map (bottom) shows that only the edge of the gap area (about 10 pixels wide) from the original LST map (top) was gap-filled by the original LST pixels, and the remaining areas were gap-filled by the reconstructed pixels..

5.4. Potential improvements

A few potential modifications could be investigated to further improve RSDAST performance. Over some scenes and conditions, if may be acceptable to use a larger spatial window (9×9 was used here) or a longer temporal window (8 days used here) to increase the sample size of valid pixels used in the reconstruction, thereby increasing the number of gap pixels that can be filled. For example, the TD time series

in Fig. 4 shows that TD has an almost constant value close to zero, so may be reasonable to extend the temporal window and use a smaller spatial window to search for valid pixel pairs. In Fig. 3, the TD variance is larger in the mountain area than in the plain, and the TD variance distribution is related with slope of the terrain. This means that the error of prediction is larger in mountain area, as demonstrated by the results from Section 4.2, so in this case it may be optimal to add more information, for example related to the slope parameter.

6. Conclusions

Remotely sensed thermal infrared imagery is affected by cloud and cloud shadows resulting in many invalid or missing LST values. In this study, a new clear sky LST reconstruction method, RSDAST, was developed based on the assumption that differences in LST between nearby pixels are relatively stable during a short time period. Using MODIS LST product, the method was applied in the northwest region of China, including Shaanxi, Ningxia, Gansu, Qinghai province, where the terrain is complicated. The reconstructed LST was evaluated using clear conditions images by masking and then reconstructing valid LST pixels. The reconstructed LST showed accuracy in flat areas with R^2 of 0.72–0.89, bias of −-0.02–0.21 K, and RMSE of 0.92–1.16 K, and for mountain areas with R^2 of 0.81–0.89, bias of −0.35−-1.52 K, and RMSE of 1.42–2.24 K.

Reconstructed LST over a plain landscape shows a better accuracy than in mountainous area, which can be explained by the theoretical assumption in the model. The algorithm yields no visible discontinuities between the clear and gap-filled regions of the reconstructed LST images. Spatial details such as the valley and ridge of the west mountain area, the Guanzhong Plain, and the river system within the plain, are preserved in the reconstructed images. In the reconstructed LST and NDVI triangle space, points distributed reasonably and correspond well to the soil moisture conditions. The model provides an effective method for filling gaps in MODIS LST images for potential spatiotemporally continuous mapping of drought.

Acknowledgments

The authors would like to thank Bin Ouyang from Chinese Academy of Agricultural Science for his contribution to this computer program. The authors would like to thank Holmes Thomas from USDA-ARS for his suggestion. This work was supported by the Natural Science Fund of China (Grants 41301457 and 41401491). USDA is an equal opportunity provider and employer.

References

Ackerman, S.A., Strabala, K.I., Menzel, W.P., Frey, R.A., Moeller, C.C., Gumley, L.E., 1998. Discriminating clear sky from clouds with MODIS. J. Geophys. Res. 103 (D24), 32141. http://dx.doi.org/10.1029/1998JD200032.

Anderson, M.C., Hain, C., Wardlow, B., Pimstein, A., Mecikalski, J.R., Kustas, W.P., 2011. Evaluation of drought indices based on thermal remote sensing of evapotranspiration over the continental United States. J. Clim. 24 (8), 2025–2044. http://dx.doi.org/10.1175/2010JCLI3812.1.

Anderson, M.C., Kustas, W.P., Alfieri, J.G., Gao, F., Hain, C., Prueger, J.H., Evett, S., Colaizzi, P., Howell, T., Chávez, J.L., 2012. Mapping daily evapotranspiration at Landsat spatial scales during the BEAREX'08 field campaign. Adv. Water Resour. 50, 162–177. http://dx.doi.org/10.1016/j.advwatres.2012.06.005.

Anderson, M.C., Hain, C., Otkin, J., Zhan, X., Mo, K., Svoboda, M., Wardlow, B., Pimstein, A., 2013. An intercomparison of drought indicators based on thermal remote sensing and NLDAS-2 simulations with U.S. drought monitor classifications. J. Hydrometeorol. 14 (4), 1035–1056. http://dx.doi.org/10.1175/JHM-D-12-0140.1.

Anderson, M.C., Zolin, C.A., Sentelhas, P.C., Hain, C.R., Semmens, K., Tugrul Yilmaz, M., Gao, F., Otkin, J.A., Tetrault, R., 2016. The Evaporative Stress Index as an indicator of agricultural drought in Brazil: an assessment based on crop yield impacts. Remote Sens. Environ. 174, 82–99. http://dx.doi.org/10.1016/j.rse.2015.11.034.

Bastiaanssen, W.G.M., Menenti, M., Feddes, R.A., Holtslag, A.A.M., 1998. A remote sensing surface energy balance algorithm for land (SEBAL): 1. Formulation. J. Hydrol. 212–213 (1–4), 198–212. http://dx.doi.org/10.1016/S0022-1694(98)00253-4.

Carlson, T.N., Gillies, R.R., Schmugge, T.J., 1995. An interpretation of methodologies for indirect measurement of soil water content. Agric. For. Meteorol. 77 (3–4), 191–205 . http://dx.doi.org/10.1016/0168-1923(95)02261-U.

Jin, M., 2000. Interpolation of surface radiative temperature measured from polar orbiting satellites to a diurnal cycle: 2. Cloudy-pixel treatment. J. Geophys. Res. 105 (D3), 4061. http://dx.doi.org/10.1029/1999JD901088.

Jin, M., Dickinson, R.E., Zhang, D.L., 2005. The footprint of urban areas on global climate as characterized by MODIS. J. Clim. 18, 1551–1565. http://dx.doi.org/10.1175/JCLI3334.1.

Khlopenkov, K.V., Trishchenko, A.P., 2007. SPARC: new cloud, snow, and cloud shadow detection scheme for historical 1-km AVHHR data over Canada. J. Atmos. Ocean. Technol. 24 (3), 322–343. http://dx.doi.org/10.1175/JTECH1987.1.

Kogan, F.N., 1995. Application of vegetation index and brightness temperature for drought detection. Adv. Sp. Res. 15 (11), 91–100. http://dx.doi.org/10.1016/0273-1177(95)00079-T.

Kogan, F.N., 1997. Global drought watch from space. Bull. Am. Meteorol. Soc. 78 (4), 621–636. http://dx.doi.org/10.1175/1520-0477(1997)078 < 0621:GDWFS > 2.0.CO;2.

Kou, X., Jiang, L., Bo, Y., Yan, S., Chai, L., 2016. Estimation of land surface temperature through blending MODIS and AMSR-E data with the bayesian maximum entropy method. Remote Sens. 8 (2). http://dx.doi.org/10.3390/rs8020105.

Li, X., Cheng, G., Liu, S., Xiao, Q., Ma, M., Jin, R., Che, T., Liu, Q., Wang, W., Qi, Y., Wen, J., Li, H., Zhu, G., Guo, J., Ran, Y., Wang, S., Zhu, Z., Zhou, J., Hu, X., Xu, Z., 2013. Heihe watershed allied telemetry experimental research (HiWATER): scientific objectives and experimental design. Bull. Am. Meteorol. Soc. 94 (8), 1145–1160. http://dx.doi.org/10.1175/BAMS-D-12-00154.1.

Lu, L., Venus, V., Skidmore, A., Wang, T., Luo, G., 2011. Estimating land-surface temperature under clouds using MSG/SEVIRI observations. Int. J. Appl. Earth Obs. Geoinf. 13 (2), 265–276. http://dx.doi.org/10.1016/j.jag.2010.12.007.

Luo, Y., Trishchenko, A.P., Khlopenkov, K.V., 2008. Developing clear-sky, cloud and cloud shadow mask for producing clear-sky composites at 250-meter spatial resolution for the seven MODIS land bands over Canada and North America. Remote Sens. Environ. 112 (12), 4167–4185. http://dx.doi.org/10.1016/j.rse.2008.06.010.

Maimaitiyiming, M., Ghulam, A., Tiyip, T., Pla, F., Latorre-Carmona, P., Halik, Ü., Sawut, M., Caetano, M., 2014. Effects of green space spatial pattern on land surface temperature: implications for sustainable urban planning and climate change adaptation. ISPRS J. Photogramm. Remote Sens. 89, 59–66. http://dx.doi.org/10.1016/j.isprsjprs.2013.12.010.

Metz, M., Rocchini, D., Neteler, M., 2014. Surface temperatures at the continental scale: tracking changes with remote sensing at unprecedented detail. Remote Sens. 6 (5), 3822–3840. http://dx.doi.org/10.3390/rs6053822.

Neteler, M., 2010. Estimating daily land surface temperatures in mountainous environments by reconstructed MODIS LST data. Remote Sens. 2 (1), 333–351. http://dx.doi.org/10.3390/rs1020333.

Sandholt, I., Rasmussen, K., Andersen, J., 2002. A simple interpretation of the surface temperature/vegetation index space for assessment of surface moisture status. Remote Sens. Environ. 79 (2–3), 213–224. http://dx.doi.org/10.1016/S0034-4257(01)00274-7.

Su, Z., 2002. The Surface Energy Balance System (SEBS) for estimation of turbulent heat fluxes. Hydrol. Earth Syst. Sci. 6 (1), 85–100. http://dx.doi.org/10.5194/hess-6-85-2002.

Sun, L., Sun, R., Li, X., Liang, S., Zhang, R., 2012. Monitoring surface soil moisture status based on remotely sensed surface temperature and vegetation index information. Agric. For. Meteorol. 166–167, 175–187. http://dx.doi.org/10.1016/j.agrformet.2012.07.015.

Sun, L., Liang, S., Yuan, W., Chen, Z., 2013. Improving a Penman–Monteith evapotranspiration model by incorporating soil moisture control on soil evaporation in semiarid areas. Int. J. Digit. Earth 6 (sup1), 134–156. http://dx.doi.org/10.1080/17538947.2013.783635.

Tobler, W.R., 1970. A computer movie simulating urban growth in the detroit region. Econ. Geogr. 46, 234. http://dx.doi.org/10.2307/143141.

Wan, Z., 1997. A physics-based algorithm for retrieving land-surface emissivity and temperature from eos/modis data. IEEE Trans. Geosci. Remote Sens. 35 (4), 980–996. http://dx.doi.org/10.1109/36.602541.

Wan, Z., Dozier, J., 1996. A generalized split-window algorithm for retrieving land-surface temperature from space. IEEE Trans. Geosci. Remote Sens. 34 (4), 892–905. http://dx.doi.org/10.1109/36.508406.

Wan, Z., Zhang, Y., Zhang, Q., Li, Z., 2002. Validation of the land-surface temperature products retrieved from Terra Moderate Resolution Imaging Spectroradiometer data. Remote Sens. Environ. 83 (1–2), 163–180. http://dx.doi.org/10.1016/S0034-4257(02)00093-7.

Westermann, S., Langer, M., Boike, J., 2011. Spatial and temporal variations of summer surface temperatures of high-arctic tundra on Svalbard - Implications for MODIS LST based permafrost monitoring. Remote Sens. Environ. 115 (3), 908–922. http://dx.doi.org/10.1016/j.rse.2010.11.018.

Xu, Y., Shen, Y., 2013. Reconstruction of the land surface temperature time series using harmonic analysis. Comput. Geosci. 61(C), 126–132. http://dx.doi.org/10.1016/j.cageo.2013.08.009.

Zhang, X., Pang, J., Li, L., 2015. Estimation of land surface temperature under cloudy skies using combined diurnal solar radiation and surface temperature evolution. Remote Sens. 7 (1), 905–921. http://dx.doi.org/10.3390/rs70100905.